

3. T. L. Wright, *U.S. Geol. Surv. Prof. Pap.* 735 (1971).
4. J. M. Rhodes *et al.*, *Eos* 64, 900 (1983); J. W. Sparks and J. M. Rhodes, *Geol. Soc. Am. Abstr. Program* 15, 692 (1983).
5. J. M. Rhodes, *J. Geophys. Res.* 88 (suppl.), A869 (1983).
6. The procedure to adjust analyses to MgO = 7.00 (percent by weight) involves the subtraction or addition of olivine of Fo_{87.5} composition [that is, containing 87.5% of the magnesian end-member (forsterite) in solid solution], the same average composition as used by Wright (3), and is described elsewhere (11, appendix).
7. J. M. Rhodes and P. W. Lipman, *Abstracts, Hawaii Symposium on Intraplate Volcanism and Submarine Volcanism* (International Association of Volcanology and Chemistry of Earth's Interior, Hilo, HI, 1979), p. 97; J. M. Rhodes, J. P. Lockwood, P. W. Lipman, *Abstracts, Generation of Major Basalt Types* (International Association of Volcanology and Chemistry of Earth's Interior—International Association of Geochemistry and Cosmochemistry, Reykjavik, Iceland, August 1982), abstr. 43.
8. J. M. Rhodes, *Eos* 64, 348 (1983).
9. ——— and J. W. Sparks, *Proc. Inst. Stud. Earth Man Conf. Open Magmatic Systems* (August 1984), p. 135 (extended abstr.).
10. J. R. Budahn and R. A. Schmitt, *Geochim. Cosmochim. Acta* 49, 67 (1985).
11. R. I. Tilling, T. L. Wright, H. T. Millard, Jr., *U.S. Geol. Surv. Prof. Pap.*, in press.
12. R. I. Tilling, *Eos* 66, 851 (1985).
13. J. P. Lockwood and P. W. Lipman, *ibid.*, in press.
14. D. C. Cox and J. Morgan, *Univ. Hawaii, Hawaii Inst. Geophys. Rep.* 77-14 (1977).
15. P. W. Lipman, *Bull. Volcanol.* 43, 703 (1980).
16. G. B. Dalrymple, E. A. Silver, E. D. Jackson, *Am. Sci.* 47, 45 (1973); D. A. Clague and G. B. Dalrymple, *U.S. Geol. Surv. Prof. Pap.*, in press.
17. D. Dzurisin and R. Y. Koyanagi, *U.S. Geol. Surv. Open-File Rep.* 81-571 (1981); D. Dzurisin, R. Y. Koyanagi, T. T. English, *J. Volcanol. Geotherm. Res.* 21, 177 (1984).
18. R. I. Tilling *et al.*, *U.S. Geol. Surv. Prof. Pap.*, in press.
19. We thank the staff members of the U.S. Geological Survey Hawaiian Volcano Observatory for support and cooperation in the sampling of the Mauna Loa eruptive products, and R. T. Helz and B. C. Hearn for constructive comments on the manuscript. Supported by NASA grant NSG-9060 and NSF grant EAR-84-18671 to J.M.R. and J.W.S.

16 June 1986; accepted 10 October 1986

Oxygen Supersaturation in the Ocean: Biological Versus Physical Contributions

H. CRAIG AND T. HAYWARD

A method based on measurements of dissolved molecular nitrogen, molecular oxygen, and argon can distinguish biological from physical contributions to oxygen supersaturation in the ocean. The derived values of biological O₂ production can be used as a check on estimates of total organic productivity measured by instantaneous rates of carbon-14 assimilation. Application to the shallow summer O₂ maxima in the North Pacific gyres shows that about 72% of the O₂ supersaturation maximum at 28°N and about 86% of the maximum at 40°N are due to net photosynthetic production.

THE MAGNITUDE OF PRIMARY PRODUCTION in the world oceans is controversial because of uncertainties in the methods of estimating productivity in the sea (1, 2). Central to this problem is the comparison of organic productivity, measured by means of instantaneous ¹⁴C uptake, with seasonal data on accumulation rates of dissolved oxygen below the surface mixed layer, and central to that comparison is a knowledge of the relative proportions of physical and biological contributions to oxygen supersaturation. We discuss here the development of the subsurface dissolved

molecular oxygen (O₂) maximum in the North Pacific gyre during summer. Reid (3) explained this maximum and its attendant O₂ supersaturation as a virtual effect caused by loss of O₂ from surface water by warming and gas exchange, leaving an induced O₂ maximum below. Shulenberg and Reid (4) later pointed out that these processes cannot account for the actual O₂ supersaturation and proposed that the major cause is photosynthetic production of O₂ below the base of the shallow mixed layer. They also concluded that productivity measured by ¹⁴C uptake in these waters was much lower than values derived from O₂ production rates, thereby initiating a debate that has continued with vigor (5–9).

We describe here a technique for precise determination of biological and physical contributions to O₂ supersaturation that is based on the use of dissolved argon (Ar) as a biologically inert surrogate for oxygen. Our method parallels a previous similar development (10) for evaluating the contributions of air injection and hydrothermal input to oceanic helium concentrations based on the use of dissolved neon (Ne) and Ar. In the present work we use molecular nitrogen (N₂) and Ar saturation anomalies to derive the contributions of air injection and net photosynthetic production to the O₂ supersaturation.

As in (10), we write the saturation anomaly for a gas as $\Delta_i = (C_i/C_i^*) - 1$, where C_i

is the observed concentration and C_i^* is the gas concentration at saturation equilibrium. The saturation anomaly is the sum of the effects of barometric pressure variations, temperature changes in the water parcel after atmospheric equilibration, air injection (by downward transport of bubbles), and, in the case of O₂, a contribution, Δ_J , from the net photosynthetic production of O₂:

$$\Delta_i(\%) = \Delta_P - 100 \left(\frac{d \ln C_i^* / dT}{C_i^*} \right) \Delta T + (\alpha^A / C_i^*) a + \Delta_J \quad (1)$$

where Δ_P is the percentage deviation of barometric pressure from 1 atm during equilibration, ΔT is the potential temperature change of the water parcel after equilibration, α^A is the volume fraction of the gas in dry air, and a is the amount of injected air in concentration units. Although, in principle, measurement of three conservative components, for example, N₂, Ar, and Ne, is necessary to define the pressure, temperature, and air injection contributions, the close similarity of Ar and O₂ solubility parameters allows precise evaluations of the air injection and Δ_J terms for O₂ to be made from measurements on N₂ and Ar. Table 1 compares the effects of air injection and temperature changes on N₂, O₂, and Ar saturation anomalies, together with the supersaturation in mixing due to the nonlinearity of C^* versus T . The effects of O₂ and Ar are essentially indistinguishable for these processes. Also shown are the relative $\beta_i D_i$ products (defined in Table 1) that govern the equilibration kinetics between bubbles and solution for the various gases (10) and that are also similar for O₂ and Ar. The primary difference is the air injection coefficient for N₂ compared with that of Ar, which can be used to evaluate the injected air component from Eq. 1 for these two gases:

$$a = 0.235 (\Delta N_2 - \Delta Ar) + 0.053 \Delta T \quad (2)$$

Table 1. N₂, O₂, and Ar saturation anomalies (Δ) for air injection and postequilibration potential temperature changes in seawater at 15°C and a salinity of 34 per mil. Row 3 gives the anomalies resulting from mixing equal parts of 10°C, 34.5 per mil and 20°C, 35 per mil seawater. Row 4 compares the products of Bunsen solubility coefficients and molecular diffusion coefficients for N₂ and O₂ in seawater at 22°C, to the same product for Ar (10). Solubility equations of Weiss (11) are used throughout.

Process	N ₂	O ₂	Ar
Air injection (1 ml/kg)	7.67%	3.75%	3.42%
$\Delta T = 1^\circ\text{C}$	1.79%	2.00%	2.01%
Mixing (10° + 20°)	0.86%	0.98%	0.94%
$(\beta D) / (\beta D)_{Ar}$ (22°C)	0.38	0.90	1

Scripps Institution of Oceanography, University of California, San Diego, La Jolla, CA 92093.

Table 2. Potential temperature (T), salinity (S), dissolved O_2 , and saturation anomalies for N_2 , O_2 , and Ar at ALCYONE stations 1 and 2. From these data are obtained the injected air component a , the O_2 anomaly due to biological effects $(\Delta O_2)_J$, and F_J , the fraction of the total O_2 supersaturation produced by photosynthesis and respiration. LT, local time.

Depth (m)	T ($^{\circ}C$)	S (per mil)	O_2 ($\mu M/kg$)	ΔO_2 (%)	ΔN_2 (%)	ΔAr (%)	a^*	$(\Delta O_2)_J$	F_J^\dagger
<i>Station 1: 28°01'N, 158°00'W (1430 LT, 29 July 1985)</i>									
2	24.82	35.471	214	3.7	2.6	-1.8	0.90	5.1	1.39
55	23.54	35.403	229	8.6	2.9	2.1	0.18	6.4	0.75
58	23.28	35.395	231	9.1	4.5	2.8	0.35	6.2	0.68
61	23.14	35.388	232	9.0	3.4	2.2	0.24	6.7	0.74
63	22.54	35.374	232	8.3	4.3	2.3	0.41	5.8	0.70
<i>Station 2: 39°50'N, 160°03'W (1300 LT, 31 July 1985)</i>									
1	18.27	33.736	246	5.1	5.2	1.1	0.96	3.6	0.72
20	15.81	33.710	266	8.3	3.9	2.2	0.41	5.9	0.72
27	14.78	33.708	278	10.8	4.5	1.3	0.76	9.3	0.86
32	13.87	33.712	288	12.7	5.3	1.4	0.91	10.9	0.86
82	10.56	33.830	265	-3.2	2.2	0.7	0.35	-4.0	1.26

*Injected air content, in milliliters (STP) per kilogram of seawater. Uncertainty for $\pm 1^{\circ}C$ change in T is ± 0.04 ml/kg. $^\dagger F_J = (\Delta O_2)_J / (\Delta O_2)_{total}$.

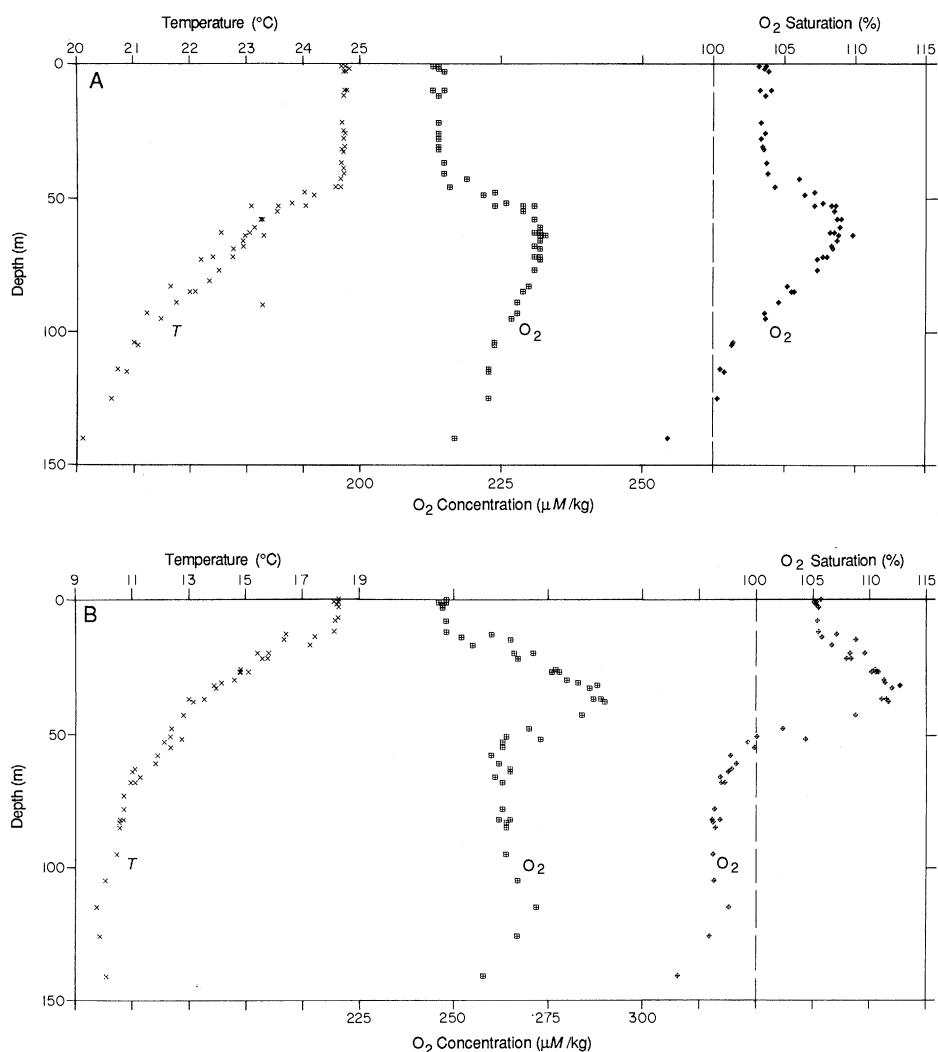


Fig. 1. Temperature (T), O_2 concentration, and O_2 saturation profiles at two stations in the upper waters of the North Pacific at $28^{\circ}N$ (A) and $40^{\circ}N$ (B) during leg 2 of the ALCYONE Expedition in August 1985. Composite data from five hydrographic casts over 10-hour periods at each station are plotted. The subsurface O_2 extrema are summer features that develop below the surface mixed layer between extrema of primary productivity (measured by instantaneous ^{14}C uptake) and of chlorophyll concentration (4).

in which the numerical coefficients (0.235 and 0.053) are derived from the tabulated $15^{\circ}C$ data (11). At $23^{\circ}C$ these coefficients are, respectively, 0.207 and 0.034, so that over the range of temperatures we are concerned with, a $1^{\circ}C$ postequilibration ΔT produces errors of only ~ 0.04 ml at standard temperature and pressure (STP) per kilogram in the calculation of the injected air component.

The $(O_2 - Ar)$ supersaturation difference, from Eq. 1, is

$$(\Delta O_2 - \Delta Ar) = \Delta_J + k_1 a + k_2 \Delta T \quad (3)$$

in which the $15^{\circ}C$ coefficients are $k_1 = 0.33$ and $k_2 = -0.014$ (Table 1). At $23^{\circ}C$, $k_2 = +0.016$, so that in the range from 15° to $23^{\circ}C$ even a $10^{\circ}C$ postequilibration ΔT produces an uncertainty of only -0.14 to $+0.16\%$ in the estimation of the O_2 production term Δ_J . Thus the effects of temperature changes in the water column are always insignificant for the evaluation of the air injection and biological O_2 components. When we evaluate the air component from Eq. 2, the biological contribution to the O_2 supersaturation in terms of the total N_2 , O_2 , and Ar saturation anomalies is

$$(\Delta O_2)_J = (\Delta O_2 - \Delta Ar) - 0.08 (\Delta N_2 - \Delta Ar) \quad (4)$$

in which the numerical coefficient varies from 0.078 to 0.081 over the range of $T = 15^{\circ}$ to $23^{\circ}C$, and the contribution of the $(N_2 - Ar)$ term is therefore always of second-order significance.

Our study of the subsurface O_2 supersaturation was carried out on leg 2 of the ALCYONE Expedition, at two stations in the North Pacific along $\sim 160^{\circ}W$. Figure 1 shows the measured temperature, O_2 , and O_2 saturation profiles. The subsurface maxima in both O_2 and ΔO_2 lie just below the base of the isothermal surface mixed layer, with the higher values of both concentration and supersaturation occurring to the north (4). At $28^{\circ}N$ (Fig. 1A) we observed a maximum ΔO_2 of 9%, compared with previously observed values of $\sim 12\%$ (3, 4, 12). At $40^{\circ}N$ (Fig. 1B) the values of ΔO_2 range up to 13%, less than the values of 20% described by Reid (3). Samples were collected in 5-liter Niskin hydrographic bottles, and O_2 was measured by titration (13). Samples for dissolved gas measurements were drawn from the Niskin bottles into 50-ml evacuated glass flasks and returned to the laboratory for analysis by gas chromatography (GC). We used a concentric dual-column technique in which all three gases could be measured without changing column temperature during the elutions (14), thus providing maximum precision for the Ar data.

The hydrographic data and N_2 , O_2 , and Ar saturation anomaly values are listed in Table 2, together with the derived quantities of a and the "biological" saturation anomaly $(\Delta O_2)_J$, as calculated from Eqs. 3 and 4. The saturation anomaly differences for $(O_2 - Ar)$ are plotted against those for $(N_2 - Ar)$ in Fig. 2, which is similar to the He-Ne-Ar plot used previously to evaluate the "excess He" component in deep waters (10). The vector for air addition lies close to the abscissa because of the large effect of air injection on N_2 supersaturation relative to the essentially identical effects on O_2 and Ar (Table 1). The net O_2 supersaturation due to photosynthesis and respiration corresponds to the increment of $(\Delta O_2 - \Delta Ar)$ above the air injection line. As noted, the air injection slope is so close to zero that the value of $(\Delta O_2)_J$ is essentially equal to $(\Delta O_2 - \Delta Ar)$. The maximum contribution from the $(\Delta N_2 - \Delta Ar)$ term in Eq. 4, in samples from the subsurface O_2 maximum is 0.16% in the 63-m sample from station 1. At this depth the total biological saturation anomaly, $(\Delta O_2)_J$, is 5.8%, so that the $(\Delta N_2 - \Delta Ar)$ term in Eq. 4 is only 0.03 of the calculated value of ΔJ . In the other samples from the subsurface maximum the fractional contribution ranges from 0.01 to 0.027 of the total ΔJ . The N_2 analyses are therefore useful for measuring the injected air component but are not essential for the calculation of the ΔJ values in this region of the North Pacific (15).

The derived $(\Delta O_2)_J$ values in Table 2 are quite consistent. At 28°N (station 1) the samples were taken over a range of 8 m in a broad O_2 maximum centered at ~60 m. The O_2 concentrations are essentially constant (range, 3 μM), and the biological contribution $(\Delta O_2)_J$ is $6.3 \pm 0.4\%$, which is 68 to 75% (average, 72%) of the total O_2 supersaturation as shown by the F_J values in Table 2. At 40°N (station 2) the subsurface O_2 maximum is much sharper, and within the range sampled (20 to 32 m) the O_2 concentration increases downward to the maximum of ~8%. About half this increase is due to the enhanced solubility with the 2°C decrease in T (Table 1), and about half is due to the increase in $(\Delta O_2)_J$, the production term, from 5.9 to 10.9% at the O_2 maximum. The $(\Delta O_2)_J$ values at the maximum, 9.3 to 10.9%, are the largest we observed, and they correspond to the maximum observed biological fraction: $F_J = 86\%$ of the total O_2 supersaturation. Thus the maximum supersaturation and maximum (net) biological production of O_2 appear to be correlated, at least in the small data set presented here. Between the O_2 maximum, at 82 m, the negative value of ΔO_2 is due to consumption of O_2 by respira-

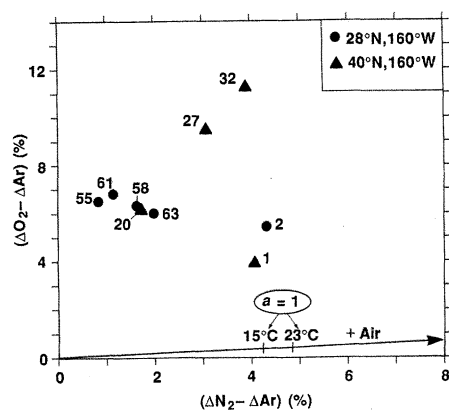


Fig. 2. The saturation anomaly difference for $(O_2 - Ar)$ plotted against the $(N_2 - Ar)$ difference. Sample depths (in meters) are shown next to the points. The line labeled "Air" is the vector for addition of air to saturated seawater at 20°C; for $a = 1$ ml (STP) per kilogram of seawater, the magnitudes of the vectors at 15° and at 23°C are indicated. For a given $(N_2 - Ar)$ difference the net O_2 saturation anomaly due to photosynthesis and respiration $(\Delta O_2)_J$ is given by the value of $(\Delta O_2 - \Delta Ar)$ relative to the air injection baseline.

tion, an effect that is greater than the net O_2 anomaly ($F_J > 1$).

Because the biological contribution is the dominant source in the O_2 maximum, the Ar saturation anomaly will normally show much less variability with depth, so that mixing with waters from above and below will tend to reduce the calculated value of F_J together with the O_2 saturation anomaly and concentration at the maximum. The calculated parameter F_J must therefore be considered as a lower limit, in the same way as the measured values of ΔO_2 and O_2 , and synoptic observations are always necessary to establish the extreme values.

Our results do not contribute directly to the comparison of oceanic productivity measured by seasonal O_2 production and by ^{14}C uptake because of the uncertainties in averaging O_2 supersaturation over depth and time and in relating ^{14}C uptake rates to net O_2 evolution (4-9). However, the seasonal O_2 accumulation calculations by both interpretations are based on the same data with a mean ΔO_2 of 8.5% at 28°N in the central gyre. Platt (5, 9) assumed that air injection accounts for 3.5% of ΔO_2 , that is, $F_J = 0.59$. Reid and Shulenberg (8) used a total ΔO_2 anomaly of $\geq 8.5\%$ for their comparison with carbon uptake. Our data from 28°N suggest that the injected air component at the O_2 maximum in this latitude amounts to ~0.33 ml/kg, corresponding to $\Delta O_2 = 1.5\%$. Another 1.5% is contributed by the combined $(\Delta P + \Delta T)$ terms, which with $(\Delta O_2)_J$ at ~6.3% produces a total O_2 supersaturation of ~9% (Table 2). Our mean $(\Delta O_2)_J$ value at 28°N is intermediate between the values adopted

by the two groups (4, 8) and (5, 9), and somewhat closer to the lower estimates.

An important problem concerning biological productivity in the North Pacific gyre can now be stated: per kilogram of seawater with a mean $(\Delta O_2)_J$ of 6% at 28°N, we observe an accumulation of 13 μM of O_2 in the ~100 days or less since stratification (8). To support this O_2 production, we require a biological uptake of at least 1 to 1.5 μM of N and ~0.06 to 0.094 μM of P, using the nominal proportionalities. These N and P requirements cannot be satisfied by seasonal changes in NO_3^- and PO_4^{3-} , since the average concentrations of these two species at and below the O_2 maximum are less than 0.2 and 0.04 $\mu M/kg$, respectively, and they do not vary with the season (16). These nutrient requirements must be maintained by vertical mixing, although it is difficult to understand the mechanism that transports nutrients through a region of essentially zero concentration extending well below the summer O_2 maximum.

Our purpose, however, is not to resolve the productivity controversy, but to introduce a method that can unambiguously define the relative effects of biological and physical contributions to O_2 supersaturation. The use of this technique to record O_2 concentration changes, together with further synoptic observations on oxygen and nutrients in the upper layers of the sea, will contribute to a realistic evaluation of the primary productivity of the oceans.

REFERENCES AND NOTES

- R. A. Kerr, *Science* **220**, 397 (1983).
- B. J. Peterson, *Annu. Rev. Ecol. Syst.* **11**, 359 (1980).
- J. L. Reid, *J. Mar. Res.* **20**, 138 (1962).
- E. Shulenberg and J. L. Reid, *Deep Sea Res.* **28**, 901 (1981).
- T. Platt, *ibid.* **31**, 1311 (1984).
- W. J. Jenkins and C. Goldman, *J. Mar. Res.* **43**, 465 (1985).
- T. Platt and W. G. Harrison, *Nature (London)* **318**, 55 (1985).
- J. L. Reid and E. Shulenberg, *Deep Sea Res.* **33**, 267 (1986).
- T. Platt and W. G. Harrison, *ibid.*, p. 273.
- H. Craig and R. F. Weiss, *Earth Planet. Sci. Lett.* **10**, 289 (1971).
- R. F. Weiss, *Deep Sea Res.* **17**, 721 (1970).
- T. Hayward, unpublished data.
- J. H. Carpenter, *Limnol. Oceanogr.* **10**, 141 (1965). Precision and accuracy are ~0.2 and 1%, respectively, for this method which is currently used by the Physical and Chemical Oceanographic Data Facility (PACODE) group of marine technicians at the Scripps Institution of Oceanography.
- The GC column (Alltech CTR-3, 6 feet by 0.25 inch) consists of two concentric 5A molecular sieve columns in which O_2 is removed from the inner column by a chemical scrubber and catalyst so that separated N_2 and Ar peaks emerge. Between these peaks a combined Ar- O_2 peak emerges from the outer column, and the outer column N_2 peak completes the sequence. The two N_2 peaks give the column split factor, and all components are then known. Typically, a 0.05-ml (STP) precise split of the gases extracted from ~30 g of seawater was transferred to the injection loop by condensation on

5A sieves at liquid nitrogen temperature, and then injected after heating for 1 minute at 100°C. Elution times for the N₂, (Ar-O₂), Ar, and outer column N₂ peaks were, respectively, 4, 9.5, 13.5, and 25 minutes at 0°C, with a flow rate of 0.03 liter/min. The analytical precision was ~0.3%, and accuracy was 0.5%. The GC values for O₂ were ~6% lower than the titration results because of bacterial consumption in the flasks and therefore were not used. When GC data for all three gases are used in Fig. 2, leakage of air into a flask moves a point parallel to the air injection slope, so that the (ΔO₂ - ΔAr) increment above the air injection baseline is unaffected. When O₂ is analyzed separately, leakage into a flask affects only N₂ and Ar, and a point in Fig. 2 moves on a vector of 130° (Table 1). This means that the (ΔO₂)_i values will always be lower limits if air leakage occurs.

15. A plot of ΔN₂ versus ΔAr provides limits on the Δ_p and Δ_T effects because the vectors for Δ_p (slope is 1) and Δ_T (slope is 0.9, 15° to 23°C) are similar to each

other, but quite different from that for air addition (slope is 2.2, 15° to 23°C). Subtracting the air component from the ΔN₂ and ΔAr values leaves the combined (Δ_p and Δ_T) anomalies ("Δ_{p,T}") for each sample, which are necessarily identical for all three gases. For the subsurface samples at 28°N, Δ_{p,T} varies from 0.7 to 1.4%, corresponding to a range in Δ_p of that same magnitude or a Δ_T range of +0.4° to 0.8°C or a combination of both effects. At 40°N the subsurface range of Δ_{p,T} is -1.7 to +0.8%, corresponding to a Δ_p of that magnitude or a Δ_T of -1° to +0.5°C or a combination. These values are not unexpected. However, the surface water values of Δ_{p,T} at 28°N and 40°N are -5.3 and -2.2% for depths of 1 to 2 m at midday. (At 28°N this effect makes $F_j > 1$.) These negative values represent bulk loss of gases that causes negative Δ_p anomalies, possibly due to cavitation from the cycloidal propellers of the R.V. *Melville*. A final effect is partial solution of gases from bubbles, which results in preferential injection of gases according to the (βD)_i

values in Table 1, that is, in a component enriched in the order of Ar, O₂, and N₂ relative to air, and thus intermediate in composition between an unfractured Δ_p component and actual air (10). In Fig. 2, partial solution of bubbles moves a point on a vector with a lesser slope than that shown for bulk air injection, so that the value of (ΔO₂)_i is slightly underestimated when the bulk air baseline is used. This effect is probably never significant for O₂, but experiments on this process would be of interest.

16. T. L. Hayward, E. L. Venrick, J. A. McGowan, *J. Mar. Res.* **41**, 711 (1983).
17. We thank J. Costello for the hydrographic and O₂ measurements aboard the R.V. *Melville*, and K. Rubin for the N₂ and Ar analyses at Scripps Institution of Oceanography; we also thank Y. Horibe and V. Craig for help both on land and at sea. Research supported by NSF grants OCE84-03111 (H.C.) and OCE85-09839 (T.H.).

17 June 1986; accepted 14 October 1986

Identification of a Juvenile Hormone-Like Compound in a Crustacean

H. LAUFER, D. BORST, F. C. BAKER, C. CARRASCO, M. SINKUS, C. C. REUTER, L. W. TSAI, D. A. SCHOOLEY

Juvenile hormone (JH) has central roles in the regulation of insect development and reproduction but has not previously been identified in other arthropod classes. The hemolymph of a crustacean, *Libinia emarginata* (Leach), has now been analyzed for JH-like compounds. Samples contained 0.003 to 0.030 nanogram of JH III per milliliter and 10 to 50 nanograms of methyl farnesoate per milliliter; methyl farnesoate is a compound structurally related to JH III that has JH bioactivity. Several tissues were examined for synthesis and secretion of JH-like compounds. Of these tissues, only the mandibular organs produced and secreted JH III and methyl farnesoate. However, microchemical analysis revealed that this JH III was racemic, and thus likely an artifactual oxidation product of methyl farnesoate. Secretion of methyl farnesoate was related to reproduction in females, with the highest rates observed in *Libinia* near the end of the ovarian cycle when oocyte growth and vitellogenesis are greatest. These results indicate that JH-like compounds such as methyl farnesoate have regulatory roles in crustaceans.

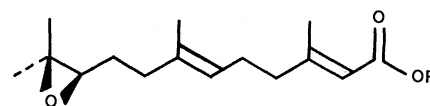
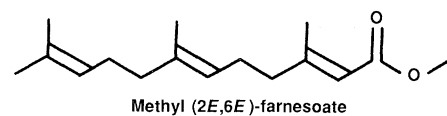
THE JUVENILE HORMONES (JHs) ARE a family of sesquiterpenoid compounds that regulate both metamorphosis and gametogenesis in insects (1). With the discovery that ecdysteroids regulate molting in both insects (2) and crustaceans (3) investigators have speculated that Crustacea might also contain a compound related to JH. This possibility is supported by the detection of JH biological activity in extracts of crustacean eyestalks (4) and data on the effects of synthetic JH analogs on crustacean metamorphosis and reproduction (5-8). These results have proven difficult to interpret, however. For example, a number of compounds that occur widely in nature have JH activity in bioassays. Thus, the juvenilizing activity found in crustacean extracts (or vertebrate and plant extracts) has generally been attributed to the presence of such compounds (9). Likewise, the high concentrations of JH analogs used in many studies with crustaceans suggest that the

observed responses may be nonspecific toxic effects.

In an attempt to identify a crustacean JH directly, we obtained hemolymph from three groups of adult spider crabs (*Libinia emarginata*): females, males, and males from which eyestalks had been removed. Acetonitrile extracts of these samples were processed (Fig. 1) and analyzed by gas chromatography-mass spectrometry (GC-MS) with selected ion monitoring (10). Extracts exhibited peaks at mass-to-charge ratios (m/z) of 76 having the same retention time as the *d*₃-methoxyhydrin derivative of JH III (Fig. 1, A and B), but no substance was detected consistently at m/z 90 with a retention time identical to that of the corresponding derivative of JH 0, JH I, or JH II. Furthermore, we were able to detect JH III acid (Fig. 1C) in the samples by using a modification of the methodology described by Bergot *et al.* (10) (see legend to Fig. 1).

We also analyzed hemolymph samples for

methyl farnesoate (MF), a compound structurally similar to JH III but lacking the epoxide moiety (see structures). MF is produced by the corpus allatum of some insect species (11-13), has JH activity (12-14), and may function as a JH at some developmental stages (12, 13). GC-MS analysis of these samples revealed the presence of a material eluting with the same retention time as MF and exhibiting peaks at m/z 69, 114, and 121 (Fig. 2) in the ratios characteristic of this compound.



The concentrations of JH-like compounds in the above hemolymph samples are shown in Table 1. The relative concentrations of these compounds were similar in each group, with MF exceeding JH III by about a factor of 1000. The lowest concentration of MF and related compounds was found in adult females; these compounds were present in about three times this concentration in hemolymph of adult males. The highest levels of these compounds (five to ten times that of the concentrations in adult females) were observed in males from which eyestalks had been removed 14 days

H. Laufer, Department of Molecular and Cell Biology, University of Connecticut, Storrs, CT 06268, and Marine Biological Laboratory, Woods Hole, MA 02543.
D. Borst, Department of Biological Sciences, Illinois State University, Normal, IL 61761.
F. C. Baker, C. C. Reuter, L. W. Tsai, D. A. Schooley, Zoon Research Institute, Palo Alto, CA 94304.
C. Carrasco and M. Sinkus, Department of Molecular and Cell Biology, University of Connecticut, Storrs, CT 06268.